Petroleum Science 23 (2026) 4842–4854

Contents lists available at ScienceDirect

Petroleum Science

journal homepage: www.keaipublishing.com/en/journals/petroleum-science

Original Paper

Physics-informed autoencoder with Bayesian optimization for real-time stuck pipe risk prediction

Mu-Chen Liu [a], Zhao-Peng Zhu [c,*], Xian-Zhi Song [b,*], Yan-Long Yang [b], Tao Pan [b], Zhi Yan [b], De-Tao Zhou [a]

[a] College of Artificial Intelligence, China University of Petroleum (Beijing), Beijing, 102249, China
[b] College of Petroleum Engineering, China University of Petroleum (Beijing), Beijing, 102249, China
[c] College of Mechanical and Transportation Engineering, China University of Petroleum (Beijing), Beijing, 102249, China

A R T I C L E I N F O

Article history:
Received 4 June 2025
Received in revised form
14 January 2026
Accepted 15 January 2026
Available online 30 January 2026

Edited by Jia-Jia Fei

Keywords:
Stuck pipe
Autoencoder
Bayesian optimization of the physics-based model
Physics-data model

A B S T R A C T

The issue of stuck pipe can significantly increase non-productive time, even leading to accidents such as drill string failure, which causes a sharp rise in drilling costs. Therefore, timely and accurate monitoring for signs of stuck pipe is crucial. This study establishes a hybrid physics-data model comprising a drag-torque model, hydraulic model, and unsupervised learning algorithm. The first model component enables real-time calibration of physical model parameters through Bayesian optimization using streaming data, achieving accurate dynamic calculations for three sticking-type characteristic parameters: theoretical hook load, theoretical torque, and theoretical pump pressure. The second component employs an unsupervised learning algorithm to monitor anomalous trends in characteristic parameters across different sticking types. Prior to real-time deployment, the model was trained on a 31-sample normal drilling dataset, with validation set sticking incidents subsequently guiding optimal threshold selection. Two field test cases demonstrate that the model's reconstruction error effectively characterizes sticking progression, triggering alerts 4 and 30 min before friction-reduction operations respectively.

This methodology addresses three critical limitations in existing approaches: (1) oversight of mechanistic distinctions among sticking types, (2) ineffective utilization of physics-based models, and (3) insufficient stuck pipe data availability for small-sample learning scenarios. The proposed framework establishes a novel paradigm for stuck pipe prediction research, enabling timely implementation of field-proven prevention and control strategies in oilfield operations.

1. Introduction

Stuck pipe remains one of the most consequential risk factors in drilling operations. Both incipient sticking symptoms and complete pipe stuck not only disrupt drilling continuity but may precipitate catastrophic drill string failures, resulting in exponentially escalating non-productive time (NPT) costs (Liu et al., 2024). Early detection of impending sticking signatures coupled with proactive remedial actions prior to total immobilization is therefore critical for maintaining drilling operational safety.

Current stuck pipe monitoring and prediction methodologies primarily encompass three categories: empirical approaches, physics-based modeling, and data-driven techniques. Empirical methods rely on field engineers' operational expertise to assess sticking risks through analysis of drilling parameter trends (hook load, torque, etc.). However, these approaches require manual specification of risk discrimination thresholds, introducing inherent subjectivity. Particularly in multi-well simultaneous monitoring scenarios, static threshold configurations often prove inadequate in balancing false alarms and missed detections across heterogeneous drilling conditions (Kaneko et al., 2024).

* Corresponding author.
E-mail address: zhuzp@cup.edu.cn (Z.-P. Zhu).
Peer review under the responsibility of China University of Petroleum (Beijing).

https://doi.org/10.1016/j.petsci.2026.01.020
1995-8226/

Nomenclature

F_i	axial force, N
q_i	drill string weight, N
α_i	inclination angle
μ_i	axial drill pipe friction factor
n_{ti}	contact force, N
Δs_i	each section length, m
M_{Ti}	torque, N·m
μ_2	circumferential drill pipe friction factor
D_{bi}	drill string diameter, m
φ	azimuthal angle
B_a	shape coefficient
γ_w	shear rate, s^{-1}
τ_w	shear force, Pa
f	friction coefficient
ρ	fluid density, kg/m^3
v	average flow velocity, m/s
Δp	pressure loss, Pa
d_{hyd}	hydraulic diameter, m
A	flow cross-sectional area, m^2
P	wetted perimeter, kg·m^{-3}
N_{ReG}	generalized Reynolds number
N_{CRG}	critical generalized Reynolds number
n_p	roughness-related parameter
ECD	equivalent circulating density, g/cm^3
ΔSPP	difference between the actual and theoretical standpipe pressure, Pa
Δp_i	the frictional pressure loss in the ith segment, Pa
h	vertical depth, m
n	flow behavior index
K	consistency coefficient, Pa·s^n
τ_y	yield stress, Pa
ε_x	relative percentage error of drilling parameters
y_x	actual measured value of the drilling parameter
$\widehat{y_x}$	estimated value from Bayesian optimization
$\boldsymbol{X}$	input variable
$\boldsymbol{Z}$	intermediate variable generated by the encoder
$\widehat{\boldsymbol{X}}$	final variable generated by the decoder
$L(\boldsymbol{X}, \widehat{\boldsymbol{X}})$	minimization objective function
L_{recon}	reconstruction error
N	the total number of discretized segments

Physics-based approaches employ established tubular mechanics and hydraulic models to compute wellbore states using real-time drilling parameters (e.g., hook load, torque) combined with static operational parameters (well trajectory, casing program, bottom-hole assembly, mud weight, etc.). These models enable theoretical calculations, such as determining theoretical hook load and torque through drag-torque modeling to infer drill string obstruction risks (Courteille et al., 1986; Lesage et al., 1988), or computing theoretical standpipe pressure via hydraulic modeling to evaluate cuttings accumulation potential (Saini et al., 2020; Zhu et al., 2022a) or through logical rules based on expert experience qualitatively determine whether there is a tendency of stuck pipe (Al Dushaishi et al., 2021; Siqueira et al., 2024). However, these physics-driven methodologies require extensive parameter inputs for accurate analysis. Critical limitations arise from either unattainable static parameters or delayed data acquisition, particularly in multi-well monitoring scenarios. Such parametric uncertainties induce persistent unquantifiable errors in simultaneous sticking risk assessments across multiple wells, ultimately compromising prediction reliability.

Recent years have witnessed substantial scholarly efforts in developing data-driven methodologies for stuck pipe prediction, primarily employing supervised and unsupervised learning paradigms. Supervised learning algorithms are trained on pre- and post-sticking drilling parameter sequences to detect analogous risk patterns in real-time data streams (Abbas et al., 2019; Kizayev et al., 2023). However, these methods frequently suffer from overfitting issues due to the inherent scarcity of labeled sticking incidents in drilling datasets (Inoue et al., 2022). In contrast, unsupervised approaches establish baseline behavioral patterns from normal drilling operations, subsequently flagging anomalous parameter deviations (Mopuri et al., 2022; Nakagawa et al., 2021). While circumventing sample scarcity constraints, such purely data-driven frameworks often produce non-physical predictions owing to the absence of domain-specific priors (e.g., mechanical constraints, hydraulic principles), resulting in elevated rates of both false positives and missed detections during field deployment (Zhu et al., 2022b).

In recent years, physics-informed machine learning methods have made significant progress in industrial applications. For example, the task-oriented physical collaboration network proposed by Shen et al. (2025b) has been successfully applied to pipeline defect detection, and the vision-language cyclic interaction model (VLCIM) developed by Shen et al. (2025a) has improved the accuracy of industrial defect detection through multimodal fusion. These methods demonstrate that integrating physical mechanisms with data-driven models can significantly enhance the reliability and interpretability of the models.

This study develops a hybrid physics-data model applicable to all drilling operational conditions (including drilling, tripping, etc.). The main innovations of this study are as follows:

(1) Hybrid framework of dynamic physics model calibration and unsupervised learning: A novel hybrid framework is proposed that integrates the drag-torque model, hydraulic model, and a Bi-LSTM autoencoder for the first time. This approach addresses the issues of overfitting in small-sample scenarios and the lack of mechanistic interpretability in pure data-driven models.
(2) Bayesian optimization for dynamic parameter calibration: Through Bayesian optimization, key uncertain parameters of the physical models (such as friction coefficient and fluid rheological parameters) are dynamically and automatically calibrated using real-time data streams. This enables accurate calculation of characteristic parameters like theoretical hook load, theoretical torque, and theoretical standpipe pressure, overcoming parameter uncertainties in multi-well monitoring.
(3) Physically interpretable feature extraction based on sticking mechanisms: Based on the mechanisms of three types of stuck pipe incidents (mechanical sticking, differential pressure sticking, and hole cleaning-related sticking), eight physically interpretable feature parameters are extracted. This breaks through the limitations of traditional single-feature monitoring.

The remainder of this paper is structured as follows: Section 2 (Methodology) details the hybrid physics-data model, including physical foundations, Bayesian optimization for dynamic calibration, feature parameter extraction, and the unsupervised learning architecture; Section 3 (Results and discussion) presents model training, validation outcomes, and performance evaluation through two field cases; finally, Section 4 (Conclusion) summarizes the key findings and suggests future research directions.

2. Methodology

The methodology is systematically organized into four integrated sections to establish a robust hybrid physics-data framework for stuck pipe prediction: Section 2.1 establishes the foundation through drilling physics-based models (drag-torque and hydraulic models) to calculate theoretical characteristic parameters. Section 2.2 introduces a dynamic calibration method using Bayesian optimization to resolve critical parameter uncertainties in real-time. Section 2.3 defines the sticking-specific feature parameters derived from calibrated model outputs, and Section 2.4 presents an unsupervised LSTM-autoencoder algorithm that monitors anomalies in these parameters to enable early risk detection.

Fig. 1 systematically delineates the end-to-end workflow of the proposed hybrid methodology from a machine learning pipeline perspective, visually summarizing the cohesive relationships and data flow across the three core phases—training, validation, and testing. The figure illustrates the seamless integration of physical principles with data-driven learning, highlighting how mechanistic models and computational algorithms interact throughout the process. The figure visually demonstrates that physics-based models, driven by Bayesian optimization, continuously supply the learning algorithm with mechanistically validated feature inputs specific to stuck pipe mechanisms, while the unsupervised learning algorithm identifies anomalous patterns within these physically-grounded features, ultimately forming a predictive framework that achieves robust physical interpretability while maintaining adaptive data-driven intelligence.

2.1. Drilling physics-based model

Stuck pipe incidents predominantly occur during tripping and drilling operations, with three primary classifications: mechanical sticking, differential sticking, and hole cleaning-related sticking. Each manifestation exhibits distinct mechanistic origins and diagnostic signatures. Mechanical sticking manifests through anomalous fluctuations or elevations in drag and torque during tubular movement. Differential pressure sticking is characterized by abrupt static friction resistance during pipe initiation phases. Hole cleaning-related sticking additionally presents with abnormal standpipe pressure surges or elevated equivalent circulating density (ECD) profiles. This multi-mechanism complexity necessitates integrated analysis through tubular mechanics and wellbore hydraulics modeling frameworks.

Current tubular force analysis predominantly relies on drag-torque modeling frameworks. This methodology calculates axial force, lateral force, torque, and drag forces through comprehensive inputs including well trajectory, casing program, BHA configuration, mud weight, and real-time drilling parameters. During sticking tendency development, hook load in tripping operations and torque in drilling/reaming operations will deviate abnormally. The analytical process involves:

(1) Computing theoretical hook load and torque values via drag-torque models.
(2) Quantifying deviations from actual measurements as characteristic parameters.

Drag-torque models are classified into soft-string and stiff-string formulations based on the consideration of tubular bending stiffness. The soft-string approach, which neglects bending stiffness, demonstrates enhanced computational efficiency through reduced parametric requirements, making it

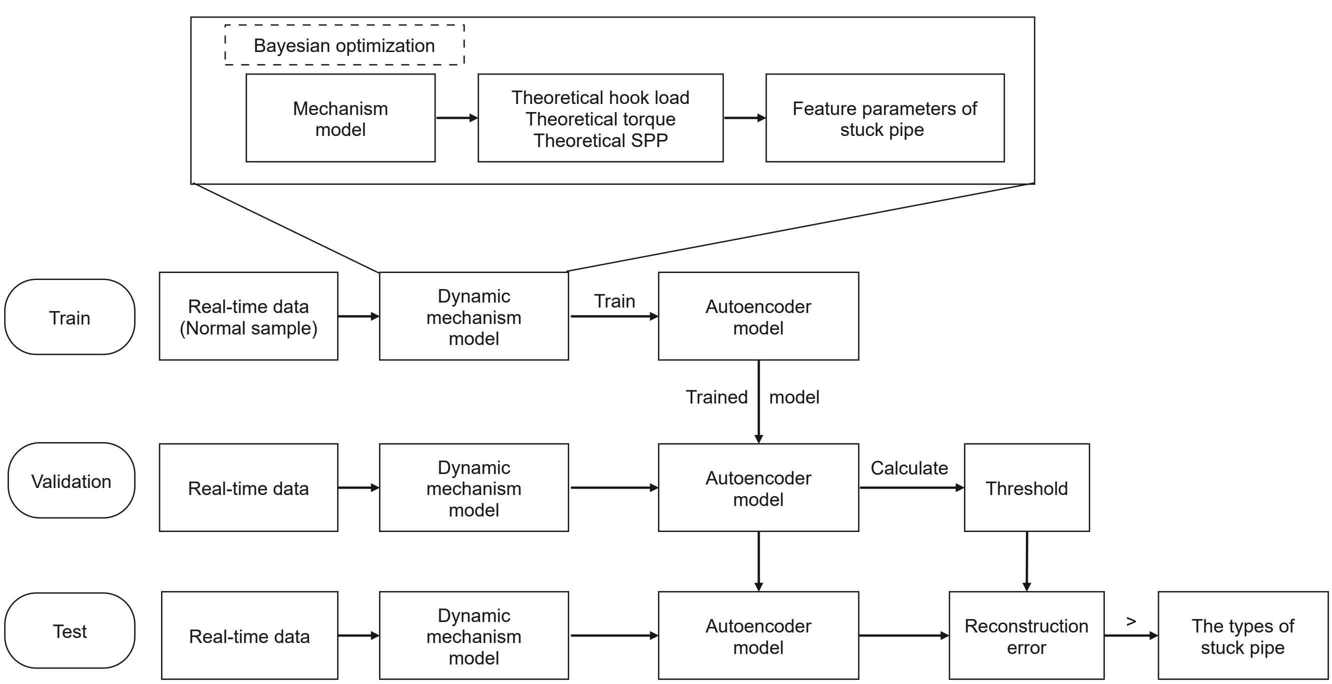

Fig. 1. Schematic diagram of the integrated methodology.

particularly suitable for real-time analytical applications. Consequently, this study adopts the soft-string formulation. The equations are expressed as follows:

$$F_i = F_{i+1} + (-q_i \cos\alpha_i \mp \mu_i \cdot n_{ti})\Delta s_i \tag{1}$$

$$M_{Ti} = \frac{1}{2}\mu_2 \cdot n_{ti} \cdot D_{bi}\Delta s_i + M_{Ti+1} \tag{2}$$

$$n_{ti} = \sqrt{(F_{i+1}\Delta\varphi \sin\alpha_i)^2 + (F_{i+1}\Delta\alpha + q\sin\alpha_i)^2} \tag{3}$$

The symbol μ_i indicates the friction coefficient between the drilling string and the wellbore at depth *i*. F_i and F_{i+1} represent the axial forces in the upper and lower parts of the drill string at depth *i*, measured in N. M_{Ti} and M_{Ti+1} represent the torque of the upper and lower sections of the drill string at depth *i*, measured in N· m. q_i, n_{ti}, Δs_i and D_{bi} respectively represent the weight (N/m), contact force with the wellbore (N/m), length (m) of the section, and outer diameter (m) of the drill string at depth *i*.

When the borehole is not clean, the circulating pressure loss of drilling fluid increases, resulting in a significant increase in the actual SPP. Therefore, the deviation between the actual and theoretical SPP are selected as mechanism parameters. This study employs the method recommended by the API (American Petroleum Institute, 2017) to calculate ΔSPP sequentially based on Eqs. (4–11).

$$B_a = \frac{(3-x)n+1}{(4-x)n}\left(1+\frac{x}{2}\right) \tag{4}$$

$$\gamma_w = \frac{8B_a v}{d_{hyd}} \tag{5}$$

$$\tau_w = \left(\frac{4-x}{3-x}\right)^n \tau_y + k\gamma_w^n \tag{6}$$

$$N_{ReG} = \frac{8\rho_{mix}v^2}{\tau_w} \tag{7}$$

$$\begin{aligned} &N_{ReG} < 3470 - 1370n,\ f = \frac{16}{N_{ReG}} \\ &3470 - 1370n < N_{ReG} < 4270 - 1370n,\ f = \frac{16N_{ReG}}{{N_{CRG}}^2} \\ &N_{ReG} > 4270 - 1370n,\ f = \frac{\frac{\log10(n_p)+3.93}{50}}{N_{ReG}^{\left(\frac{1.75-\log10(n_p)}{7}\right)}} \end{aligned} \tag{8}$$

$$\Delta p_i = \frac{2f\rho v^2}{d_{hyd}} \tag{9}$$

$$ECD = \rho + \frac{\Delta p_i}{hg} \tag{10}$$

$$\Delta SPP = SPP_{real} - \sum_{i=0}^{N}\Delta p_i \tag{11}$$

where B_a is a shape coefficient (dimensionless); x is a geometry-related parameter (dimensionless); n is the flow behavior index (dimensionless); γ_w is the wall shear rate (s^{-1}); v is the mean flow velocity ($m\cdot s^{-1}$); d_{hyd} is the hydraulic diameter (m); τ_w is the shear stress (Pa); τ_y is the yield stress (Pa); k is the consistency index ($Pa\cdot s^n$); N_{ReG} is the generalized Reynolds number (dimensionless); ρ is the density of the circulating/mixed fluid ($kg\cdot m^{-3}$); f is the Darcy friction factor (dimensionless); N_{CRG} is the critical generalized Reynolds number (dimensionless); n_p is a roughness-related parameter (dimensionless); Δp_i denotes the frictional pressure loss in the *i*th segment (Pa); ECD is the equivalent circulating density ($kg\cdot m^{-3}$); h is the vertical depth (m); g is the gravitational acceleration ($m\cdot s^{-2}$); ΔSPP is the difference between the measured and the theoretical standpipe pressure (Pa); SPP_{real} is the measured standpipe pressure (Pa); and N is the total number of discretized segments (dimensionless).

2.2. Dynamic calibration method

2.2.1. Uncertainty analysis of the physics-based model

Pipe weight serves as the pivotal parameter in drag-torque modeling calculations, directly determining the accuracy of drag and torque estimations. However, real-time BHA data acquisition remains technically challenging, forcing reliance on design specifications or manual field reporting-practices that introduce substantial uncertainties and hinder fully automated multi-well monitoring systems. Compounding these challenges, prolonged drilling operations (including tripping, slide drilling, etc.) induce cumulative pipe wear, progressively degrading model fidelity. Consequently, field engineers must perform a time-intensive manual calibration process prior to friction-drag model implementation. This involves iteratively adjusting tubular weight parameters until theoretical hook load profiles align with field measurements, thereby calibrating inherent modeling inaccuracies before conducting formal analyses (Shahri et al., 2018). Such human-intensive calibration becomes operationally prohibitive when scaling to real-time monitoring of 30+ wells simultaneously.

This critical gap underscores the urgent need for intelligent autonomous calibration frameworks to ensure continuous model accuracy across entire drilling fleets. The friction factor (typically ranging 0.1–0.6 dimensionless) quantifies tubular-to-wellbore interaction resistance, serving as a critical yet unobservable parameter in friction-drag modeling. Since real-time measurement remains technically unfeasible, field engineers must either empirically estimate this factor or derive it through post-hoc inversion calculations by matching theoretical hook load profiles with field measurements. This empirical calibration process introduces unquantifiable uncertainties, compounded by the parameter's inherent interdependence with tubular weight estimation errors. This parameter calibration process exhibits analogous uncertainty propagation characteristics to tubular weight estimation, resulting in coupled errors that are intrinsically indistinguishable. The inherent parameter interdependence fundamentally precludes precise isolation and quantification of individual error sources, severely compromising model diagnostic capabilities.

From Eqs. (1) and (3), it is mathematically demonstrated that as the well inclination angle increases, the term $q_i \cos\alpha_i$ decreases and n_{ti} increases, indicating axial force errors become predominantly governed by friction factor inaccuracies. Conversely, decreasing inclination angles amplify the influence of $q_i \cos\alpha_i$ and reduce n_{ti}, shifting error dominance to pipe weight factor uncertainties. This pattern can also be observed in Fig. 2. Fig. 2(a) shows the well inclination angles distribution of a certain well, Fig. 2(b) presents the hook loads under different friction factors, and Fig. 2(c) illustrates the hook loads under different pipe weight factors. Consequently, vertical wells require broader pipe weight factor

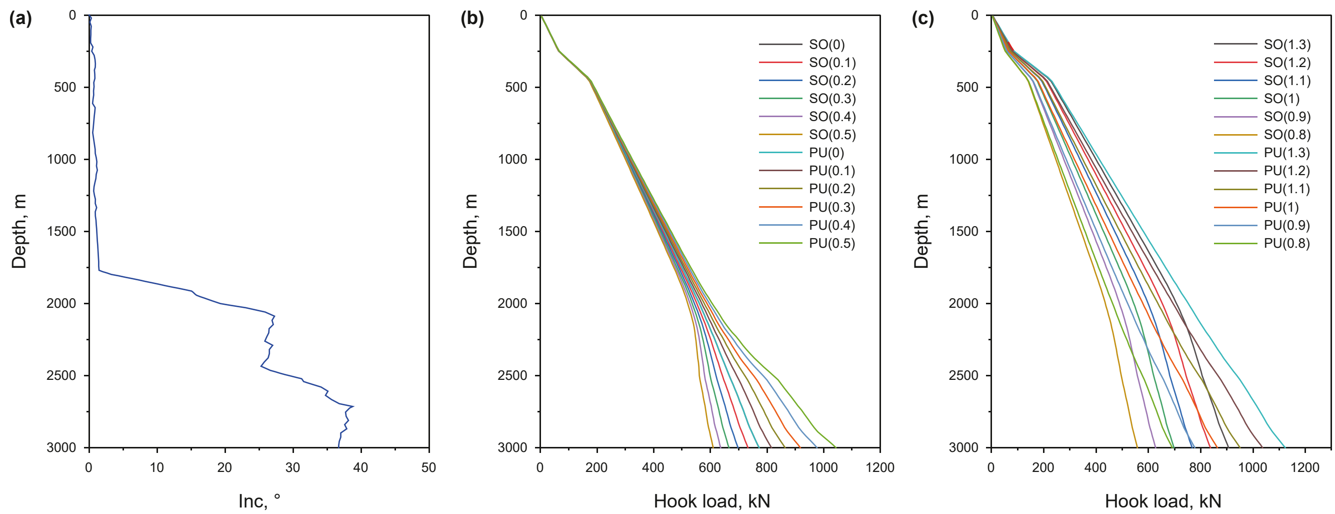

Fig. 2. Schematic diagram of drag-torque model error.

calibration ranges, whereas horizontal well sections demand extended friction factor calibration domains.

In wellbore hydraulics modeling, the flow behavior index (n, dimensionless) typically ranges from 0.6 to 0.9 in field applications, while the consistency coefficient (K, Pa·s^n) generally falls between 0.2 and 2 Pa·s^n. The yield stress (τ_y, Pa) exhibits significant operational variability from 0.001 to 20 Pa. Optimal calibration of these parameters enables:

(1) Enhanced cuttings transport capacity
(2) Reduced circulation pressure losses
(3) Minimized wellbore erosion risks
(4) Mitigated pressure surge-induced losses/kicks

However, real-time measurement of n-K-τ_y values remains technically unfeasible, forcing reliance on empirical estimation through offset well analysis or historical data extrapolation. This heuristic approach introduces substantial uncertainties, particularly in complex lithology formations where parameter interdependencies amplify systemic errors.

Furthermore, uncertainties in parameters such as pipe cross-sectional area and drilling fluid density (1–2 g/cm^3) contribute to hydraulic modeling inaccuracies. However, the limited inter-well variability of these parameters mitigates their error impacts: Pipe dimensions are selected from standardized API 5DP specifications, resulting in <5% cross-sectional area variance across wells. Mud density fluctuations remain constrained within ±0.15 g/cm^3.

Consequently, these parametric uncertainties can be effectively accounted for through the dynamic calibration process of n-K-τ_y values via lumped uncertainty compensation mechanisms, where the dominant rheological parameters of n-K-τ_y inherently absorb secondary error components during real-time model calibration.

2.2.2. Bayesian optimization

Both drag-torque and hydraulic models exhibit regime-specific computational frameworks, necessitating precise operational state identification. Friction-drag modeling requires distinct formulations for tripping out (hook load calculation), tripping in (hook load), reaming (torque analysis), and drilling (torque prediction). Hydraulic computations are only executed during pump activation phases (circulating conditions). Real-time drilling involves more than 10 distinct operational regimes, making automated regime identification imperative for accurate stuck pipe risk monitoring. Prior to conducting automated model calibration using real-time data, the selection of calibration data points must adhere to three critical operational constraints:

(1) Non-anomalous parameter trajectories: Data must originate from normal drilling operations without impending sticking signatures.
(2) Maximum temporal threshold: Prolonged time lags induce model distortion through depth-dependent parameter sensitivity variations and static parameter mismatch.
(3) Minimum temporal threshold: Immediate data inclusion risks pattern contamination from incipient abnormal trends and transient equipment fluctuations.

The calibrated physical models under these constraints establish accurate baseline behavioral profiles for sticking-free operations. Therefore, how to define and select normal data is crucial. To achieve automatic calibration of the mechanism model, the length of the periodic calibration time window is of great significance. The selection of the calibration time window length needs to match the average cycle time of sticking events from their initiation to the development stage and finally to drill string sticking. In this way, it can be ensured as far as possible that the data points automatically selected for periodic calibration meet the above three requirements.

Through statistical analysis of existing drill string sticking data samples, sticking primarily occurs during tripping operations, with some cases occurring during drilling operations. In tripping operations, from the onset of abnormal fluctuations in friction resistance to on-site detection of sticking trends and subsequent drill string movement operations, most events occur within 5 stands, with an average duration of 20–30 min, as shown in Fig. 3. Sticking events during drilling operations often manifest as sudden torque surge events with shorter cycles, typically within 3 min. Therefore, to ensure the significance of model calibration, the calibration time window is set to 30 min. Meanwhile, to avoid noise from single data points affecting model performance, the average value within the preceding 3 min of the data point is used as the valid value for calibrating model parameters. Since real-time data may include all drilling conditions, if the verification data

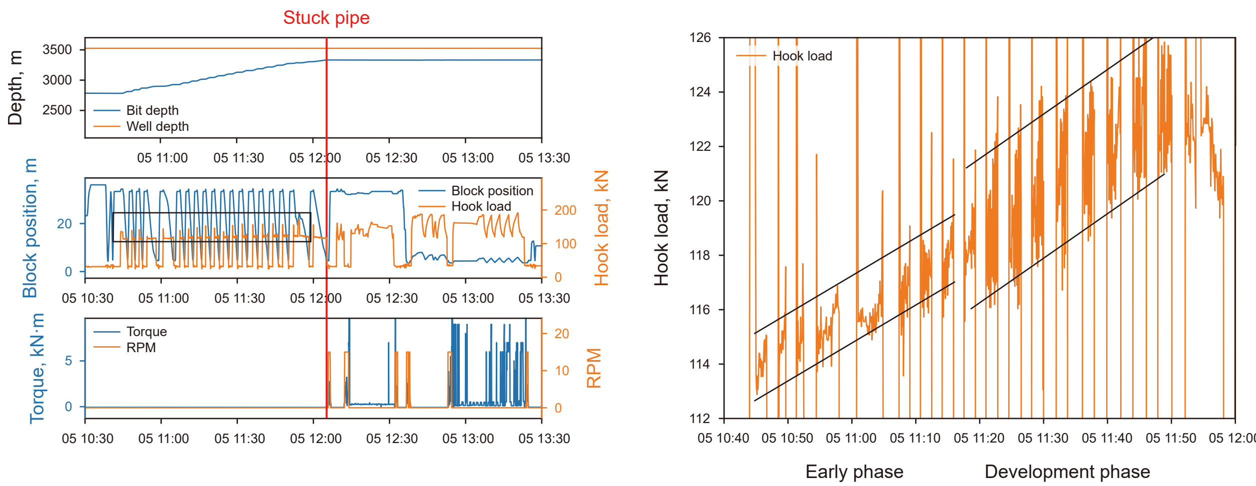

Fig. 3. Real time data during stuck pipe (early stage, middle stage, complete sticking).

points are unsuitable for calibrating the hydraulic model (e.g., when pumps are not activated) or the drag-torque model (e.g., when the hook load is empty and does not represent the true axial force at the wellhead), the calibration data points are sequentially postponed until suitable data points for calibration are obtained. It is worth noting that before calibrating the drag-torque model, the hook load must first be subtracted by the weight of the block to obtain the effective hook load value.

Both the calibration of hydraulic models and string mechanics models exhibit two distinct characteristics. First, they have a strong mechanistic nature, with complex response relationships between each parameter and the model's calculation results, though certain physical laws exist—for example, a larger friction coefficient leads to higher torque. Therefore, they are not suitable for stochastic optimization algorithms such as genetic algorithms or particle swarm optimization (Rezaee Jordehi, 2014). Instead, the evaluation results of the model after each set of calibration parameters should be rationally utilized as prior knowledge to provide directional guidance for the optimization of the next set of parameters.

Bayesian optimization (Greenhill et al., 2020) establishes a surrogate function (probabilistic model) based on historical evaluation results of the objective function to find the minimum of the objective function. The difference between the Bayesian method and random or grid search lies in that it uses previous evaluation results as reference when attempting the next set of hyperparameters, thus avoiding many futile attempts. This is highly consistent with the requirements of this task. The simple process of Bayesian optimization is as follows:

(1) Initialization: Randomly select several parameter sets x, train the model, and obtain the corresponding model evaluation metrics ε_x.
(2) Surrogate function fitting: Use a surrogate function (e.g., Gaussian process) to fit the relationship between x and y (where y represents the evaluation metric).
(3) Optimal parameter selection: Use an acquisition function to select the optimal x*.
(4) Model evaluation: Input x* into the model to obtain new y, then return to Step 2.

where the evaluation function is given by Eq. (12).

$$\varepsilon_x = \left| \frac{(y_x - \widehat{y_x})}{y_x} \right| \times 100\% \tag{12}$$

In the equation, ε_x represents the relative percentage error of drilling parameters, y_x is the actual measured value of the drilling parameter, $\widehat{y_x}$ is the estimated value from Bayesian optimization, and x denotes the drilling parameters, which can be hook load, torque, and standpipe pump pressure.

The Bayesian optimization routine is tasked with calibrating the critical uncertain parameters of the physics-based models to minimize the disparity between theoretical predictions and field measurements. For the drag-torque model, the targeted parameters are the friction coefficient (μ) and the pipe weight factor. For the hydraulic model, the parameters are the rheological properties of the drilling fluid: the flow behavior index (n), the consistency coefficient (K), and the yield stress (τ_y). The physical guidance of this process is manifested through two primary mechanisms. The objective function is to minimize a physically meaningful error metric, namely the relative percentage error ε_x (Eq. (12)) between the measured (y_x) and theoretically calculated ($\widehat{y_x}$) values of key drilling parameters (hook load, torque, standpipe pressure). This ensures the optimization is inherently driven by the principle of physical consistency. Constrained search space: The optimization

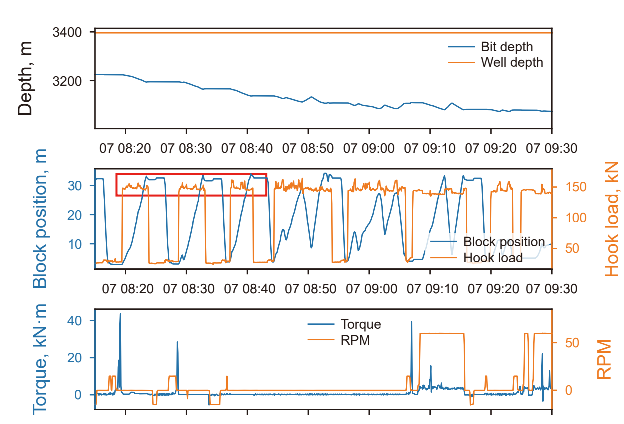

Fig. 4. Abnormal fluctuations in dynamic friction.

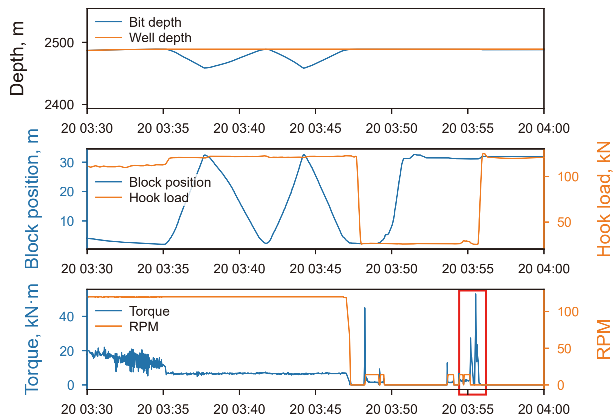

Fig. 5. Binding torque.

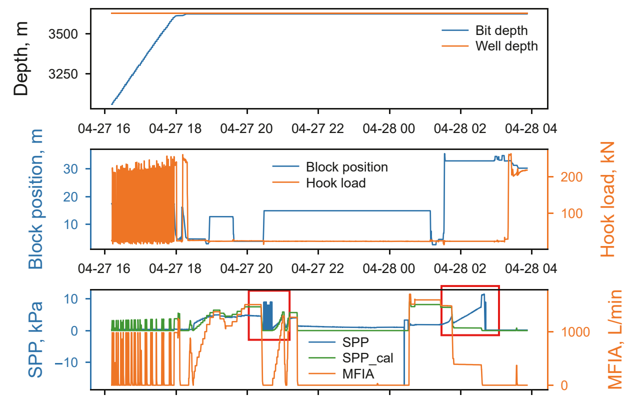

Fig. 7. Schematic diagram of abnormal pump pressure fluctuations and pump pressure buildup.

is conducted within pre-defined, physically plausible bounds for each parameter. For instance, the friction coefficient μ is bounded between 0.1 and 0.6, a range encompassing typical downhole conditions. These constraints are derived from operational experience and engineering standards, preventing the convergence towards non-physical solutions.

This approach contrasts with black-box optimization, as it leverages domain knowledge to guide the search efficiently, ensuring the calibrated models remain both accurate and physically interpretable.

2.2.3. *Sticking characteristic parameters*

Stuck pipe incidents are categorized into three primary types based on mechanistic origins: mechanical sticking, differential pressure sticking, and hole cleaning-related sticking. The distinct mechanistic origins, characteristic parameters, and temporal evolution patterns exhibited by different types of stuck pipe incidents necessitate the application of hydraulic and tubular mechanics models to compute type-specific critical parameters. This methodology enables precise detection of developing sticking patterns unique to each category.

Mechanical sticking incidents are primarily attributed to well trajectory irregularities and borehole constriction, manifested through abnormal frictional drag and torque fluctuations during tripping operations. As evidenced in Figs. 4 and 5, these events are characterized by three diagnostic parameters: the deviation between theoretical and measured hook loads, the deviation between theoretical and measured torque, and variance in dynamic friction fluctuations.

The main cause of differential sticking is that the wellbore pressure is significantly higher than the formation pressure, leading to a tendency for wellbore fluid to flow into the formation. When the pipe string is stationary, this tendency can adsorb the string onto the wellbore wall, thereby hindering the movement of the string. Moreover, the longer the stationary time, the greater the likelihood of differential pressure sticking occurring (Sampaio and Lourenco, 2013). As evidenced in Fig. 6, differential pressure sticking is mainly manifested as excessively high static friction and torque at the moment of startup when the pipe string transitions from rest to motion (for example, at the initial moment of tripping out, the hook load significantly exceeds the average hook load during movement, while at the initial moment of tripping in, it falls significantly below that average) (Inoue et al., 2024). The corresponding characteristic parameters can be summarized as starting static friction, starting static torque, and stationary time.

The main cause of hole cleaning-related is that cuttings generated during drilling are not timely removed, leading to accumulation in the wellbore and hindering pipe string movement. Compared with mechanical sticking, this type of sticking is also characterized by abnormal fluctuations and increases in pump pressure (Payrazyan and Robinson, 2023), as shown in Fig. 7. Therefore, the corresponding characteristic parameters are the difference between theoretical and actual standpipe pump pressure and the variance of abnormal fluctuations in actual standpipe pump pressure. The theoretical values of these parameters are all calculated by a dynamic calibration model, which defines the

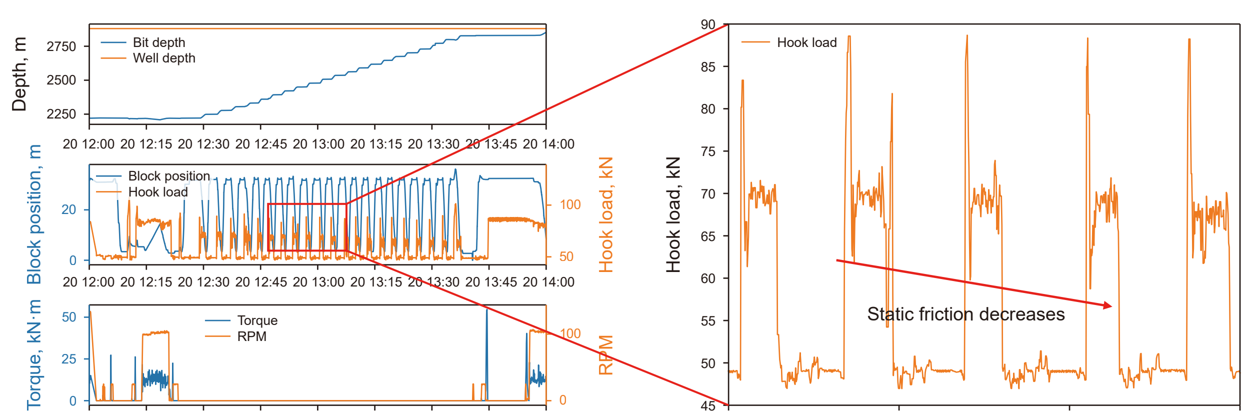

Fig. 6. Starting static friction.

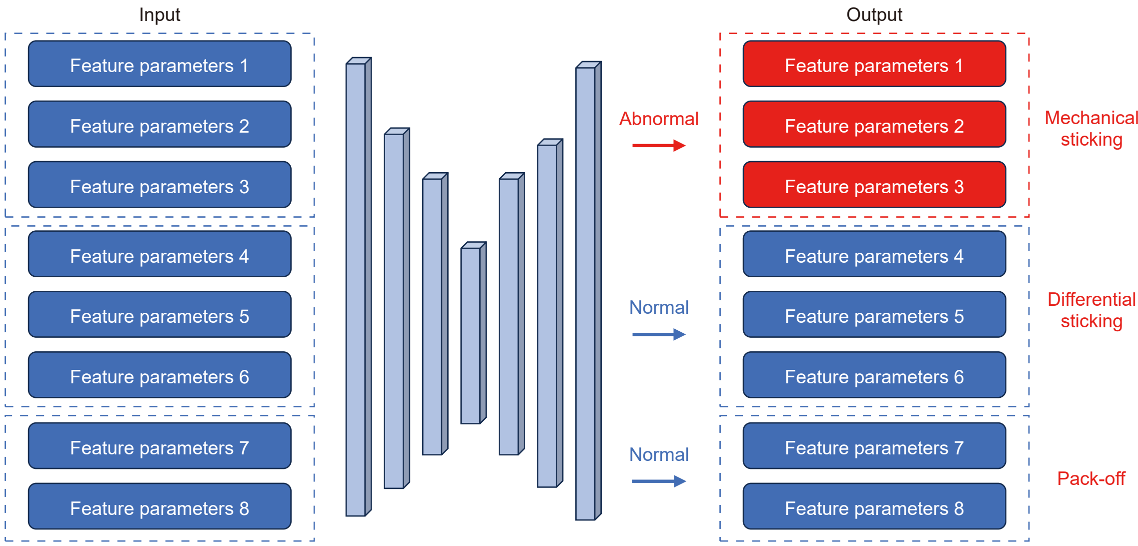

Fig. 8. Model structure diagram.

normal values of the parameters. Table 1 shows all the characteristic parameters.

2.3. Unsupervised learning algorithm

2.3.1. Model principle

Unsupervised learning, a machine learning approach, analyzes unlabeled drilling data to detect anomalies indicating sticking risks. By autonomously identifying patterns in normal operations, it extracts intrinsic data features without requiring pre-labeled risk markers. This enables real-time detection of abnormal parameter deviations. The methodology bypasses dependency on scarce labeled incidents while adapting dynamically to evolving drilling conditions. Unlike supervised approaches that require precisely annotated stuck-pipe labels—a task complicated by the scarcity of incidents and ambiguous temporal boundaries in risk onset identification. This leads to the problem that supervised learning algorithms are prone to overfitting. Therefore, unsupervised learning is more suitable for this scenario.

Unsupervised learning algorithms encompass clustering methods, dimensionality reduction techniques, and autoencoder (Dike et al., 2018). Autoencoders, widely applied in anomaly detection and feature extraction, operate by compressing input sequences to capture intrinsic temporal dynamics, followed by reconstruction through a decoder. Abnormal patterns are identified through elevated reconstruction errors resulting from deviations in learned normal behavior. Temporal autoencoders excel at extracting sequential dependencies in drilling time-series data, making them particularly suited for stuck-pipe prediction. The LSTM-based variant employs long short-term memory networks as both encoder and decoder components (Fig. 8). During training, the model minimizes reconstruction loss (Eqs. (14–17)) to learn latent representations of normal drilling parameter evolution, effectively isolating anomalies when applied to real-time data streams.

$$\boldsymbol{Z} = LSTMEncoder(\boldsymbol{X}) \tag{13}$$

$$\widehat{\boldsymbol{X}} = LSTMDecoder(\boldsymbol{Z}) \tag{14}$$

$$L(\boldsymbol{X}, \widehat{\boldsymbol{X}}) = \frac{1}{T}\sum_{t=1}^{T} \|x_t - \widehat{x}_t\|^2 + \alpha \cdot \|\boldsymbol{z}\|^2 \tag{15}$$

$$L_{\text{recon}} = \frac{1}{T}\sum_{t=1}^{T} \|x_t - \widehat{x}_t\|^2 \tag{16}$$

where $\boldsymbol{X}$ is the input variable, $\boldsymbol{Z}$ is the intermediate variable generated by the encoder, $\widehat{\boldsymbol{X}}$ is the final variable generated by the decoder, $L(\boldsymbol{X}, \widehat{\boldsymbol{X}})$ is the minimization objective function of the training process of the temporal autoencoder, and α is the regularization coefficient. L_{recon} is the reconstruction error in the model monitoring process and is an important basis for judging whether there is a risk of stuck pipe, as shown in Fig. 7.

2.3.2. Alarm threshold

A critical implementation challenge of LSTM autoencoders lies in the manual determination of alert thresholds, where reconstruction errors exceeding predefined values trigger sticking

Table 1
The feature parameters of the three types of stuck pipe.

Number	Stuck type	Feature parameters
1	Mechanical sticking	The difference between the theoretical hook load and the actual hook load
2		The difference between the theoretical torque and the actual torque.
3		The variance of abnormal fluctuations in dynamic friction.
4	Differential sticking	Starting static friction
5		Starting static torque
6		Stationary time
7	Hole cleaning-related sticking	The difference between the actual SPP and the theoretical SPP
8		The variance of abnormal fluctuations in actual SPP

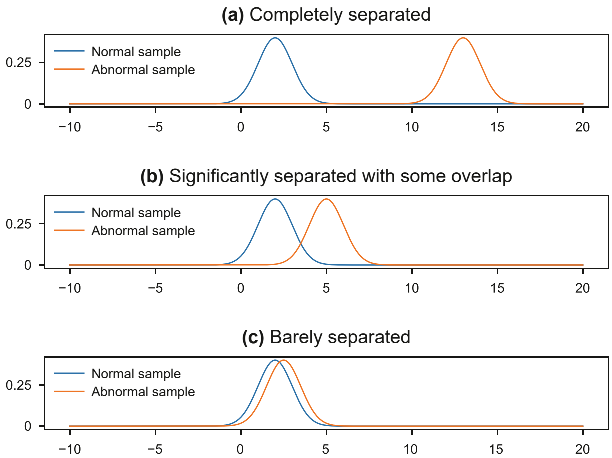

Fig. 9. The distribution of reconstruction errors between normal samples and diamond samples.

alarms. Arbitrary threshold selection risks either excessive false alarms (thresholds too sensitive) or dangerous missed detections (thresholds too lenient). This study proposes a "missed detection priority" strategy grounded in risk asymmetry analysis: Field investigations demonstrate that undetected stuck pipe incidents can escalate into catastrophic consequences including drill string failures, wellbore abandonment, and non-productive time. The potential economic losses, safety risks and time costs are much higher than the short-term efficiency losses caused by false alarms, which conforms to the basic logic of the asymmetry of risk consequences.

The distinct classification characteristics between reconstruction errors of normal samples and stuck pipe incidents necessitate threshold determination through validation set analysis to prioritize minimized missed detections. By statistically analyzing the frequency distribution of reconstruction errors in validation sets containing both normal and sticking samples, this study ensures significant separability between the two categories. Typically, normal samples exhibit compact quasi-normal distributions characterized by small means and standard deviations, whereas stuck pipe incidents produce broader distributions with substantially larger means and variances, forming distinguishable bimodal patterns. As illustrated in Fig. 9(a–c), three distinct scenarios emerge: complete separation (non-overlapping distributions), partial overlap (distinct peaks with transitional zones), and non-separation (indistinguishable unimodal distribution). The proposed methodology focuses on scenarios with clear separability, setting thresholds at the inflection point between normal and abnormal clusters to ensure early risk detection while maintaining operational feasibility.

For cases (a) and (b), the threshold can be set as,

$$threshold_{\mathrm{a}} = \max\left(L_{\mathrm{recon\_normal}}\right) \tag{17}$$

$$threshold_{\mathrm{b}} = \min\left(L_{\mathrm{recon\_abnormal}}\right) \tag{18}$$

where, $L_{\mathrm{recon\_normal}}$ is the reconstruction error of normal samples in the validation set, and $L_{\mathrm{recon\_abnormal}}$ is the reconstruction error of stuck pipe samples in the validation set.

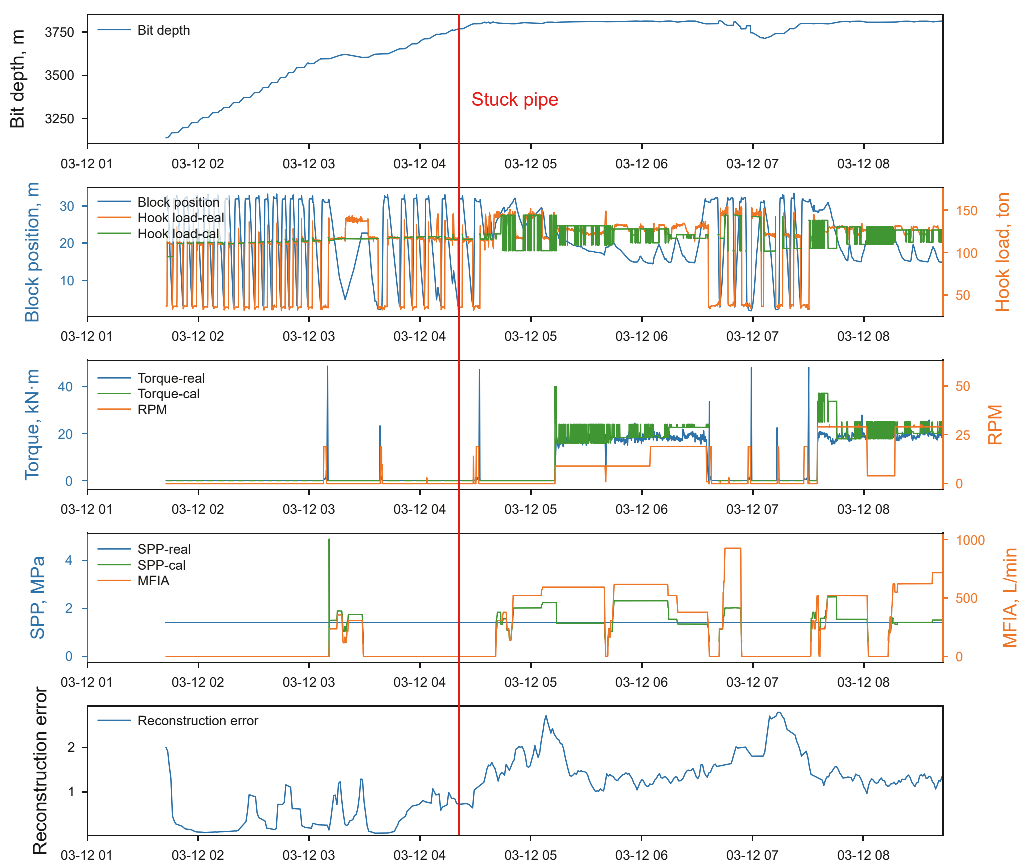

Fig. 10. The reconstruction error of the validation well.

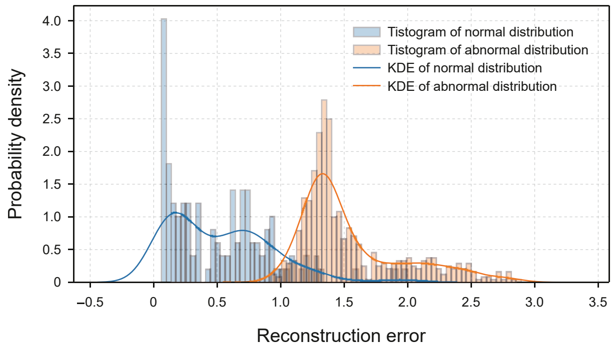

Fig. 11. The reconstruction error statistics of the validation well.

2.4. Dataset description

The dataset employed in this study comprises 46 oil wells (37 onshore and 9 offshore) across Chinese oilfields, documenting 51 stuck pipe incidents (45 during tripping operations, 6 during drilling operations). The dataset incorporates real-time drilling parameters, well trajectory measurements, bottom-hole assembly configurations, casing programs, and drilling fluid properties. For model development, training data were selected from non-sticking operational periods of 28 incident wells and 3 normal wells. Validation and testing sets were constructed using 1 well and 14 wells respectively.

It is important to note that the proposed model employs an unsupervised learning strategy. Consequently, the training phase utilizes exclusively normal drilling data to establish a baseline model of non-anomalous operations. The model learns to reconstruct the temporal patterns of normal operations optimally. Therefore, it is never exposed to or trained on labeled stuck pipe events during this phase. This design fundamentally avoids the overfitting problem commonly associated with supervised learning on imbalanced datasets where fault samples are scarce. The dataset provides millions of high-frequency data points recorded throughout the complete drilling lifecycle—from initial spud-in to final well completion—and encompasses diverse well types from both onshore and offshore operations. This extensive and varied dataset captures a wide spectrum of normal drilling behaviors and operational conditions, thereby enabling the model to learn a robust and generalized representation of expected downhole dynamics.

3. Results and discussion

3.1. Model training and validation

The methodology initiates with dynamic calibration of physics-based models through simulation tracking of training well data, enabling real-time computation of stuck pipe characteristic parameters. An unsupervised LSTM autoencoder is subsequently trained on these parameters to learn normal operational patterns. Fig. 10 illustrates reconstruction error trends from a validation well, where errors remained stable below 1.0 during normal operations, with transient spikes caused by localized dynamic friction anomalies. Pre-sticking and post-sticking phases exhibited sustained error escalation, reaching up to 2.9 at most, which was significantly higher than the reconstruction error during the normal period. Threshold determination via Eq. (18) utilized probability distribution analysis of validation set errors (Fig. 11), employing kernel density estimation (KDE) and histogram visualization (Hamzi et al., 2025). The reconstruction errors during the normal period and the stuck drilling period partially overlap. Therefore, the model alarm threshold should use Eq. (18), where $L_{\mathrm{recon\_normal}}$ is 0.93, and thus the threshold is set to 0.93.

3.2. Performance comparison with baseline models

To further verify the superiority of the proposed hybrid physics-data model for stuck pipe prediction, this section compares its performance with five representative models covering three mainstream technical paradigms (pure physics-based, pure data-driven, and hybrid models). The comparison is conducted under unified experimental conditions to ensure fairness, with metrics focusing on both early warning effectiveness and engineering practicality. The detailed information of the models is shown in Table 2.

The comparative analysis employed four selected evaluation metrics to provide a comprehensive assessment of model performance from both technical and operational perspectives. All models were evaluated on the same test set across both onshore and offshore environments. The testing protocol ensured temporal separation between training and test data to prevent data leakage.

(1) Accuracy: Overall correctness in identifying normal and stuck conditions
(2) False alarm rate (FAR): Percentage of normal operations incorrectly flagged as abnormal

Table 2
Detailed information of models.

Model category	Model name	Structure settings
Physics-based	Drag-torque model	Friction coefficient $\mu = 0.3$ (fixed value); parameters such as wellbore trajectory and drill string weight adopt a set of default values
	Empirical rule model	Hook load deviation $>\pm 15\%$ of normal value, torque surge $>50\%$ of average value, SPP fluctuation >5 MPa; thresholds are fixed for all well sections.
Data-driven	LSTM	Supervised learning framework; 3-layer LSTM (hidden dimension = 128) + 1 fully connected output layer; loss function: Binary cross-entropy; optimized via Adam optimizer (learning rate = 1e-3).
	Random forest	Supervised learning framework; 100 decision trees, maximum depth = 8 (optimized via 5-fold cross-validation); input features are raw drilling parameter time series.
	LSTM autoencoder	Unsupervised learning framework; network structure: 2-layer LSTM encoder + 2-layer LSTM decoder (hidden dimension = 64); input features are raw drilling parameter time series.
Hybrid (physics + data)	Physics-informed LSTM autoencoder	Unsupervised learning framework; network structure: 2-layer LSTM encoder + 2-layer LSTM decoder (hidden dimension = 64); input features are physical parameter time series.

Table 3
Detailed information of models.

Model category	Model name	Accuracy, %	FAR, %	MDR, %	AEWT, min
Physics-based	Drag-torque model	68.5	31.2	31.5	8.5
	Empirical rule model	72.3	27.5	27.7	10.1
Data-driven	LSTM	83.7	16.1	16.3	16.8
	Random forest	80.5	19.3	19.5	14.2
	LSTM autoencoder	85.4	14.5	14.6	18.7
Hybrid (physics + data)	Physics-informed LSTM autoencoder	92.5	7.3	7.5	22.5

(3) Missed detection rate (MDR): Percentage of actual stuck incidents that were not detected
(4) Average early-warning time (AEWT): Mean time advance between first alarm and stuck occurrence

Based on the comprehensive performance metrics detailed in Table 3, the proposed physics-informed LSTM autoencoder demonstrates unequivocal superiority across all evaluated dimensions, achieving a remarkable 92.5% accuracy that represents a 24.0% absolute improvement over pure physics-based models and a 7.1% enhancement over pure data-driven approaches, thereby establishing new benchmarks in predictive precision for stuck pipe early warning systems. The model's exceptional reliability is further evidenced by its significantly reduced false alarm rate (7.3%) and missed detection rate (7.5%), representing 50%–76% improvements over baseline models, while its 22.5-min average early warning time provides a critical 34%–165% extension in operational response window compared to conventional methods. These performance advantages stem from the novel integration of mechanistic modeling with data-driven intelligence. Bayesian optimization enables dynamic calibration of physical parameters to overcome static empirical limitations; physics-derived feature parameters replace raw data inputs to enhance interpretability and noise robustness, and the unsupervised architecture eliminates dependency on scarce labeled incidents.

3.3. Case test results

The trained model with validation-calibrated thresholds was evaluated on test wells, with Fig. 12 illustrating the real-time monitoring outcomes from the first test well during a tripping-in operation. The data captured a critical progression: At 12:00, consecutive drill stand movements exhibited an 8-ton reduction in measured hook load, accompanied by a gradual increase in reconstruction errors due to rising friction difference. By 12:05, the reconstruction error exceeded the predefined threshold of 0.93, triggering an automated alert. Field crews recognized the obstruction at 12:09 and initiated reaming operations to mitigate

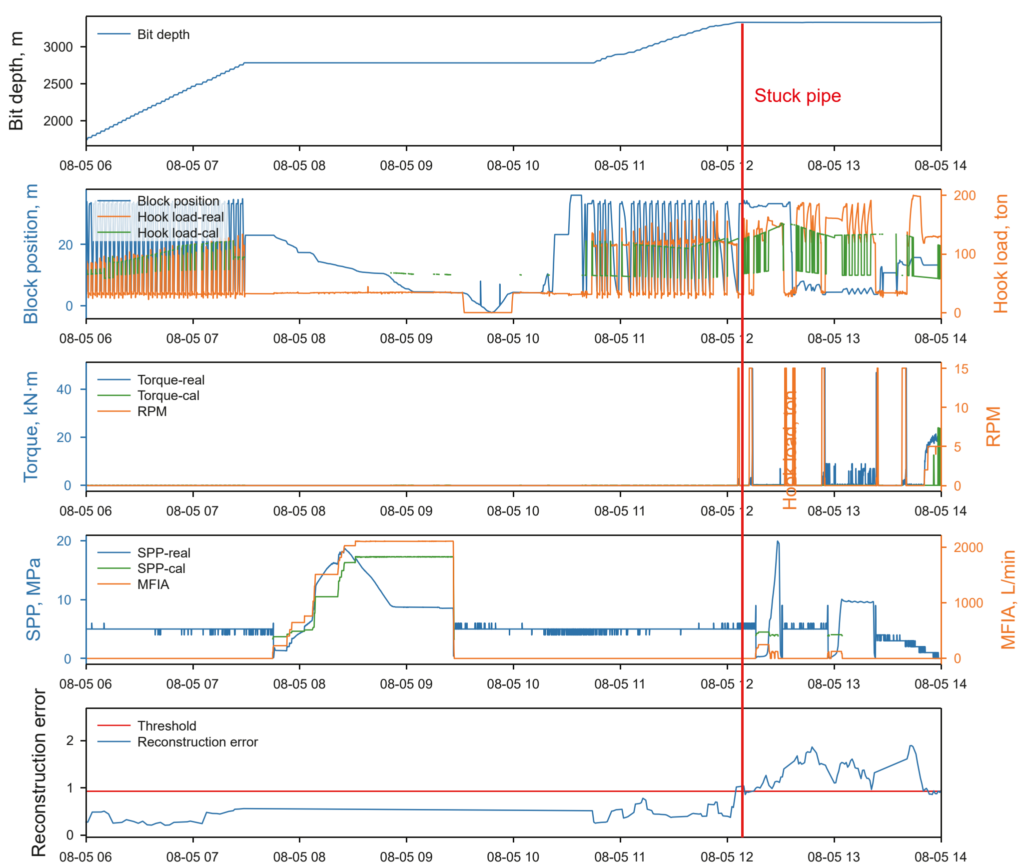

Fig. 12. Case 1.

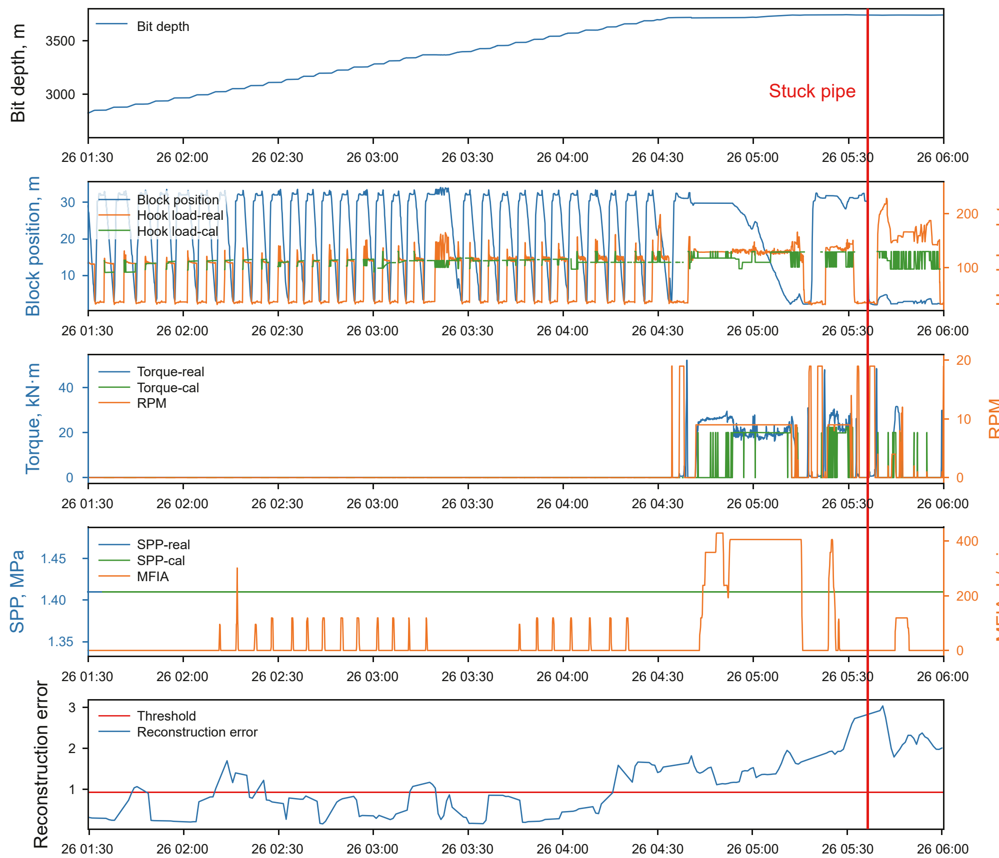

Fig. 13. Case 2.

friction, during which pump activation revealed significant pressure blockage anomalies, with the actual standpipe pump pressure deviating from theoretical values by up to 16.8 MPa. Subsequent overpull attempts escalated the hook load to 199 tons, further amplifying reconstruction errors. Notably, the model generated alerts during the second consecutive anomalous drill stand movement, providing a 4-min advance warning prior to manual field intervention.

Fig. 13 presents 6 h of real-time tripping-in data encompassing pre- and post-sticking phases for the first test well. Due to missing standpipe pressure measurements, the physical model's calculated pump pressure was aligned with theoretical values, and consequently, standpipe pump pressure analysis was excluded from the autoencoder framework. During the pre-sticking phase (1:45–3:20), multiple drill stands exhibited abnormal dynamic friction fluctuations indicative of impending sticking risks. Corresponding reconstruction error spikes exceeded the 0.93 threshold at 1:45, 2:30, and 3:10, triggering valid alerts. A systematic latency of 3–5 min was observed between parameter deviation onset and model response, attributable to computational delays inherent in time-series feature extraction. From 4:30 to 5:30, sustained hook load anomalies and torque surging signaled progressive risk escalation. The critical sticking incident occurred at 5:40 with a 228-ton overpull event, prompting reaming operations. While reconstruction errors breached the threshold at 4:15, the definitive diagnostic signature emerged post-5:00 through cumulative error amplification. This temporal progression provided a 30-min early warning window prior to manual intervention, demonstrating the model's capability to detect latent risk patterns despite data gaps.

4. Conclusions

This study proposes a hybrid stuck-pipe prediction model integrating drilling physics-based models with unsupervised learning algorithms. Two field test cases demonstrate the model's capability to accurately characterize sticking progression through reconstruction error monitoring, triggering alerts 4 and 30 min prior to the implementation of friction-reduction measures, respectively.

At a dynamic calibration frequency of 30 min, the model achieves optimal parameter fidelity with balanced false-positive/false-negative rates. However, current sampling mechanisms are vulnerable to extreme outliers during transient drilling anomalies, inducing calibration drift and transient false alarms. Future implementations will integrate robust regression techniques to mitigate outlier influence, enhancing model stability.

Moreover, future research could also focus on predictive classification of stuck pipe types through reconstruction error decompxosition (e.g., friction-dominated vs. hydraulics-driven anomalies), facilitating targeted mitigation measures.

CRediT authorship contribution statement

Mu-Chen Liu: Writing – original draft, Visualization, Validation, Methodology, Formal analysis. **Zhao-Peng Zhu:** Supervision, Formal analysis. **Xian-Zhi Song:** Supervision, Project administration. **Yan-Long Yang:** Writing – original draft, Visualization, Data curation. **Tao Pan:** Validation, Software. **Zhi Yan:** Visualization, Validation. **De-Tao Zhou:** Validation, Methodology.

Declaration of competing interests

The authors declare that they have no known competing financial interests or personal relationships that could have appeared to influence the work reported in this paper.

Acknowledgments

The authors gratefully acknowledge the support of National Science Fund for Distinguished Young Scholars (52125401) and National Key Research and Development Project of China (2019YFA0708300).

References

Abbas, A.K., Dawood, J., 2019. Application of machine learning approach for intelligent prediction of pipe sticking. In: International Petroleum Exhibition and Conference. https://doi.org/10.2118/197396-MS.

Al Dushaishi, M.F., Abbas, A.K., Alsaba, M., Abbas, H., Dawood, J., 2021. Data-driven stuck pipe prediction and remedies. Upstream Oil Gas Technol. 6, 100024. https://doi.org/10.1016/j.upstre.2020.100024.

American Petroleum Institute, 2017. Rheology and Hydraulics of Oil-well Drilling Fluids, seventh ed. Massachusetts Avenue NW.

Courteille, J.M., Fabre, M., Hollander, C.R., 1986. An advanced solution: The drilling adviser. J. Petrol. Technol. 38 (8), 899–904. https://doi.org/10.2118/12072-PA.

Dike, H.U., Zhou, Y., Deveerasetty, K.K., Wu, Q., 2018. Unsupervised learning based on artificial neural network: A review. In: 2018 IEEE International Conference on Cyborg and Bionic Systems (CBS), pp. 322–327. https://doi.org/10.1109/cbs.2018.8612259.

Greenhill, S., Rana, S., Gupta, S., Vellanki, P., Venkatesh, S., 2020. Bayesian optimization for adaptive experimental design: A review. IEEE Access 8, 13937–13948. https://doi.org/10.1109/access.2020.2966228.

Hamzi, B., Hutter, M., Owhadi, H., 2025. Bridging algorithmic information theory and machine learning: Clustering, density estimation, Kolmogorov complexity-based kernels, and kernel learning in unsupervised learning. Phys. Nonlinear Phenom. 476, 134669. https://doi.org/10.1016/j.physd.2025.134669.

Inoue, T., Nakagawa, Y., Kaneko, T., Wada, R., Abe, S., Yasutake, G., 2024. A novel approach of machine learning incorporating physical knowledge of hook load for early stuck detection. In: Offshore Technology Conference Asia. https://doi.org/10.4043/34930-MS.

Inoue, T., Nakagawa, Y., Wada, R., Miyoshi, K., Abe, S., Kuroda, K., Nishi, M., Bilen, H., Mopuri, K.R., 2022. Early stuck detection using supervised and unsupervised machine learning approaches. In: Offshore Technology Conference Asia. https://doi.org/10.4043/31376-MS.

Kaneko, T., Inoue, T., Nakagawa, Y., Wada, R., Abe, S., Yasutake, G., Fujita, K., 2024. Hybrid approach using physical insights and data science for stuck-pipe prediction. SPE J. 29 (2), 641–650. https://doi.org/10.2118/218013-PA.

Kizayev, T., Irawan, S., Khan, J.A., Khan, S.A., Cai, B., Zeb, N., Wayo, D.D.K., 2023. Factors affecting drilling incidents: prediction of suck pipe by XGBoost model. Energy Rep. 9, 270–279. https://doi.org/10.1016/j.egyr.2023.03.083.

Lesage, M., Falconer, I.G., Wick, C.J., 1988. Evaluating drilling practice in deviated wells with torque and weight data. SPE Drill. Eng. 3 (3), 248–252. https://doi.org/10.2118/16114-PA.

Liu, M., Song, X., Zhu, Z., Li, G., Xiao, H., Fu, L., Pan, T., Li, X., Yang, Y., 2024. Inertial effect of drill pipe friction trend and early warning of stuck pipe. In: SPE Annual Technical Conference and Exhibition. https://doi.org/10.2118/220991-ms.

Mopuri, K.R., Bilen, H., Tsuchihashi, N., Wada, R., Inoue, T., Kusanagi, K., Nishiyama, T., Tamamura, H., 2022. Early sign detection for the stuck pipe scenarios using unsupervised deep learning. J. Petrol. Sci. Eng. 208, 109489. https://doi.org/10.1016/j.petrol.2021.109489.

Nakagawa, Y., Inoue, T., Bilen, H., Mopuri, K.R., Miyoshi, K., Abe3, S., Wada, R., Kuroda, K., Tamamura, H., 2021. An unsupervised learning model for pipe stuck predictions using a long short-term memory autoencoder architecture. In: SPE Asia Pacific Oil and Gas Conference and Exhibition. https://doi.org/10.2118/205677-MS.

Payrazyan, V.K., Robinson, T.S., 2023. Leveraging targeted machine learning for early warning and prevention of stuck pipe, tight holes, pack offs, hole cleaning issues and other potential drilling hazards. In: Offshore Technology Conference. https://doi.org/10.4043/32169-MS.

Rezaee Jordehi, A., 2014. Particle swarm optimisation for dynamic optimisation problems: A review. Neural Comput. Appl. 25 (7–8), 1507–1516. https://doi.org/10.1007/s00521-014-1661-6.

Saini, G.S., Ashok, P., van Oort, E., 2020. Predictive action planning for hole cleaning optimization and stuck pipe prevention using digital twinning and reinforcement learning. In: IADC/SPE International Drilling Conference and Exhibition. https://doi.org/10.2118/199548-MS.

Sampaio, J.H.B., Lourenco, A., 2013. A hybrid model for predicting the likelihood of differential sticking in offshore wells. In: Offshore Technology Conference Brasil. https://doi.org/10.4043/24462-MS.

Shahri, M., Wilson, T., Thetford, T., Nelson, B., Behounek, M., Ambrus, A., D'Angelo, J., Ashok, P., 2018. Implementation of a fully automated real-time torque and drag model for improving drilling performance: Case study. In: SPE Annual Technical Conference and Exhibition. https://doi.org/10.2118/191426-MS.

Shen, X., Li, L., Ma, Y., Xu, S., Liu, J., Yang, Z., Shi, Y., 2025a. VLCIM: A vision-language cyclic interaction model for industrial defect detection. IEEE Trans. Instrum. Meas. 74, 1–13. https://doi.org/10.1109/TIM.2025.35183364.

Shen, X., Liu, J., Ren, Y., Jiang, L., Wang, L., Zhao, H., Li, R., 2025b. A task-oriented physical collaborative network for pipeline defect diagnosis in a magnetic flux leakage detection system. Comput. Ind. 169, 104290. https://doi.org/10.1016/j.compind.2025.104290.

Siqueira, V.S.D.M., Cuadros, M.A.S.L., Munaro, C.J., De Almeida, G.M., 2024. Expert system for early sign stuck pipe detection: Feature engineering and fuzzy logic approach. Eng. Appl. Artif. Intell. 127, 107229. https://doi.org/10.1016/j.engappai.2023.107229.

Zhu, N., Huang, W., Gao, D., 2022a. Numerical analysis of the stuck pipe mechanism related to the cutting bed under various drilling operations. J. Petrol. Sci. Eng. 208, 109783. https://doi.org/10.1016/j.petrol.2021.1019783.

Zhu, S., Song, X., Zhu, Z., Yao, X., Liu, M., 2022b. Intelligent prediction of stuck pipe using combined data-driven and knowledge-driven model. Appl. Sci. 12 (10), 5282. https://doi.org/10.3390/app12105282.